Palaeomagnetism of the loess/palaeosol sequence in Viatovo (NE Bulgaria) in the Danube basin

Diana Jordanova, Jozef Hus, Jordan Evlogiev, Raoul Geeraerts

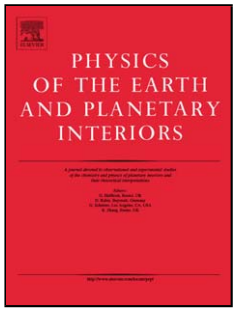

Title: Palaeomagnetism of the loess/palaeosol sequence in Viatovo (NE Bulgaria) in the Danube basin

Authors: Diana Jordanova, Jozef Hus, Jordan Evlogiev, Raoul Geeraerts

PII: S0031-9201(08)00032-0
DOI: doi:10.1016/j.pepi.2008.02.008
Reference: PEPI 4900

To appear in: *Physics of the Earth and Planetary Interiors*

Received date: 16-1-2007
Revised date: 12-2-2008
Accepted date: 13-2-2008

Please cite this article as: Jordanova, D., Hus, J., Evlogiev, J., Geeraerts, R., Palaeomagnetism of the loess/palaeosol sequence in Viatovo (NE Bulgaria) in the Danube basin, *Physics of the Earth and Planetary Interiors* (2007), doi:10.1016/j.pepi.2008.02.008

Palaeomagnetism of the loess/palaeosol sequence in Viatovo (NE Bulgaria) in the Danube basin.

Diana Jordanova (1), Jozef Hus (2), Jordan Evlogiev (3), Raoul Geeraerts (2)

(1) Geophysical Institute, Bulgarian Academy of Sciences, Acad. G. Bonchev Str., Sofia, Bulgaria, e-mail: vanedi@geophys.bas.bg
(2) Centre de Physique du Globe de l'IRM, 5670 Dourbes, Belgium, e-mail: jhus@oma.be
(3) Geological Institute, Bulg. Acad. Sci., Acad. G. Bonchev Str., bl. 24, 1113 Sofia, Bulgaria

Abstract

The results of a palaeomagnetic investigation of a 27m thick loess/palaeosol sequence in Viatovo (NE Bulgaria) are presented in this paper. The sequence consists of topsoil S_0, 7 loess horizons (L_1-L_7) and 6 interbedded palaeosols (S_1-S_6) overlying a red clay (terra rossa) complex. Magnetic viscosity experiments, IRM acquisition, AMS analysis and NRM stepwise alternating and thermal demagnetisation experiments of pilot samples were implemented for precise determination of the characteristic remanence and construction of a reliable magnetostratigraphical scheme. Analysis of IRM acquisition curves using the expectation - maximization algorithm of Heslop et al. (2002) suggests that the best fitting is obtained by three coercivity components. Component 1 corresponds to SD maghemite/magnetite, while component 2 is probably related to the presence of oxidised detrital magnetites. The third component shows varying coercivities depending on the degree of pedogenic alteration of the samples and probably reflects the presence of detrital magnetite grains oxidised at different degree.

The relevance of the Viatovo section as a key representative sequence for the loess cover in the Danube basin is confirmed by the presence of geomagnetic polarity changes in the lower part of the sequence. The youngest one recorded in the seventh loess unit L_7 can be identified as corresponding to the Matuyama/Brunhes palaeomagnetic polarity transition. Two normal magnetozones were found in the red clay complex, probably corresponding to the Jaramillo and Olduvai subchronozones of the Matuyama chron.

Key words: loess-palaeosol, viscous remanence, IRM acquisition, IRM component unmixing, magnetostratigraphy, Matuyama/Brunhes boundary, Jaramillo and Olduvai subchronozones, Bulgaria.

1. Introduction

Palaeomagnetism is one of the rare methods for chronostratigraphical correlation and dating of Middle and Upper Pleistocene loess/palaeosol sediments, mainly because of the time limits of other dating techniques and the lack of micro- and macrofaunal findings with dating significance. The latter is particularly the case with the Viatovo sequence examined below (Evlogiev, 2006). Indeed, other dating methods: amino acid racemification (Wehmiller and Miller, 2000), thermoluminescence (Forman et al., 2000, Singhvi et al., 2001), Optically Stimulated Luminescence (Huntley et al., 1985; Hutt et al., 1988) and radiocarbon (Trumbore, 2000) dating are limited in time. On the other hand, records of geomagnetic field reversals such as the position of the Matuyama/Brunhes (M/B) polarity reversal and the possible presence of "excursions" or short-term reversals within the Matuyama and Brunhes chrons are important stratigraphic markers. Especially significant is the contribution of palaeomagnetism to a reliable stratigraphic correlation of the East European loess deposits, in particular in the

Danube basin because of the varying sources of aeolian dust, differences in geomorphological relief and climate gradients (Pye, 1987). Investigations of the loess-palaeosol sediments from the Northern Black Sea coastal area by Dodonov et al. (2006) identified the Matuyama/Brunhes boundary at the base of pedocomplex S_7. Nawrocki et al. (2002) found the M/B transition in the sequence of Zahvizdja (East Carpathian Foreland) in an interglacial soil, equivalent to oxygen isotope stage 19. In the Western Black Sea area, Tsatskin et al. (2001) and Gendler et al. (2006) discovered the same polarity boundary respectively between pedocomplexes PK6 and PK7 in Roxolany and in the upper part of PK7 in Novaya Etuliya. The aim of the present study is to establish a reliable magnetostratigraphy of the loess-palaeosol sediments in the low Danube area through detailed rock magnetic (Jordanova et al. 2007) and palaeomagnetic investigations of the Viatovo sequence.

2. Loess cover in Bulgaria and site description.

The recent geomorphological relief in North Bulgaria is blanketed by widespread loess deposits. Loess-palaeosol sequences of various thickness and age occur on certain palaeogeomorphological forms: the Pliocene Denudation Surface (PDS); the Old Abrasive-Accumulative Level (OAAL); Pleistocene river terraces T_6, T_5, T_4, T_3, T_2, T_1, T_0^1 and the Holocene terrace T_0 (Fig. 1a). Each of them has a typical lithology and stratigraphic position (Evlogiev, 1993).

The oldest palaeogeomorphologic form, PDS, in North Bulgaria was shaped during the Pliocene along the shore of the Dacian lake basin. It is characterised by an undulating to flat relief in lower Cretaceous limestones and sandstones at an absolute altitude of 200–250m. In the study area, in Viatovo, a number of palaeokarsts assumed to be of Albian age developed and were buried subsequently by kaolinitic sands. The complete sedimentary

sequence on the PDS form above the kaolinitic level in this region consists of red clays and a loess/palaeosol sequence of 8 loess horizons and 7 palaeosols according to Evlogiev (2006). The second geomorphologic unit, the OAAL, was formed at the beginning of the Biber glacial about 2.59 Ma ago, by cold invasion and intensification of neo-tectonic movements. As a result, significant hydrological changes occurred. In the realm of the Dacian basin these changes were dominated by erosional incision that sculpted the OAAL relief. Its absolute height is 70-90 m and it is sloping towards the Danube River. The OAAL consists of two facies in the area of Russe: a basal gravel-sand complex (dated at 2.59 - 1.06 Ma) covered by a gravel-clay complex (1.06 - 0.84 Ma). The ages mentioned are deduced from fauna, magnetostratigraphy and geochronology (Evlogiev, 2006). A complete loess/palaeosol complex developed above the fluvio-lacustrine sediments, or the two gravel-clay complexes. The number of loess and palaeosol units on the seven river terraces $T_6 - T_0$[1] depends strongly on the age of the terrace formation. Six loess units occur on T6 but only one on T_1.

The Viatovo loess/palaeosol sequence in NE Bulgaria is exposed in the walls of a quarry that was opened for extraction of kaolin (Fig. 1b). Palaeosols and loess units that could be recognised in the field were numbered and are designated respectively S_1, S_2….and L_1, L_2…The sequence consists of topsoil S_0, 7 loess horizons (L_1 - L_7) and 6 interbedded palaeosols ($S_1 – S_6$) resting on a red clay (terra rossa) complex. In the sampling area, the recent soil S_0 was truncated by quarry activities and only the lower part was preserved, characterised by its dark gray colour and prismatic structure. The upper three palaeosols ($S_1 – S_3$) are dark brown in colour, becoming gradually more reddish towards the bottom part of the units. Abundant reddish crotovinas (burrows) perforate the uppermost soil horizon. A prismatic structure is typical for the middle part of the soil units. Their lower parts are rich in $CaCO_3$ nodules, reaching sizes of a few centimetres in the bottom of S_2. Palaeosols $S_4 – S_6$ show a brown-reddish to brown-pinkish colour, have a compact clayey prismatic structure

and contain $CaCO_3$ concretions of different sizes (up to 5cm) in their bottom parts. The first loess unit L_1 shows signs of secondary pedogenic alterations. Its colour is dark brown and it has a granular structure with $CaCO_3$ coatings. Crotovinas,several centimetres in size, are visible over the whole unit and increase in number and size in its lower part. The least altered loess unit is L2, yellowish in colour and with abundant $CaCO_3$ specks. Loess unit L_3 is affected by pedogenic alteration, brown in colour and with abundant $CaCO_3$ spots. The thickness of unit L_4 is only 50cm and it consists of brown-reddish crumbly loess with large $CaCO_3$ blocks. Unit L_5 is more powdery loess with $CaCO_3$ spots that are locally highly concentrated and with red crotovinas in the bottom part. The sixth loess unit L_6 is brown-pinkish in its upper part and becomes brown and more clayey in depth. Dark brown crotovinas are visible over the whole unit. Loess unit L_7 shows also signs of severe weathering. It is brown reddish to brown pinkish in colour, clayey and contains $CaCO_3$ spots. Downward, it becomes yellowish with large brown reddish veins of clayey silt that occupy about 30% of the total surface in a vertical section. The red clays in the bottom part of the sequence, reaching a total thickness of 5.6m, have a prismatic structure with shiny black Mn coatings on the fractures. Horizontal $CaCO_3$ lenses (5 to 10cm thick and 20 to 40cm long) occur at about 2.9 m below the top of the red clay complex, which are further down replaced by red clay mixed with large irregular $CaCO_3$ blocks. The bottom part of the sequence, ending at the kaolin level, is compact yellow sandy clay with some $CaCO_3$ lenses.

3. Methods

The complete sequence has been sampled in four non-overlapping sections. Section 1 includes: topsoil S_0, first loess unit L_1, first palaeosol unit S_1 and units L_2, S_2 and L_3. Section 2 covers units S_3, L_4, S_4, L_5, S_5 and L_6. Section 3 contains palaeosol S_6 and the underlying loess unit L_7. The fourth section cuts 5.60 m through the red clays down to the kaolin level. The

vertical sections were cut deeply in the walls of the pit in order to reach fresh, non exposed material. As the main units could be followed easily along the walls of the pit (Fig. 1b) and the whole sequence was sampled in only four vertical sections, the risk of overlapping and/or sampling gaps could be avoided. Hence, the total thickness of the complete composite section after adding the four sections is 27m. In total, 275 oriented cylindrical samples (sampling interval of 10cm) for palaeomagnetic analysis were obtained with a hand-held piston driven, split corer, specially designed for the purpose. The corer was driven horizontally in the sediment and the cores oriented with a clinometer, solar and magnetic compass, in the same way as it is commonly done for hard rocks. Mechanical disturbance was minimized as the core (2.5cm in diameter and about 7cm long) can be recuperated by opening the two halves of the corer. Close to section 1, another parallel section encompassing S_0, L_1, S_1, L_2 and S_2 was sampled additionally with a narrower sampling interval of 5cm for verification of the presence (or absence) of the Blake event.

Moreover, two decimetre-sized oriented block samples were cut in all the units and loose samples taken from the whole sequence with a sampling interval of 5cm for, respectively, anisotropy of magnetic susceptibility (AMS) measurements and rock magnetic analysis. Remanent magnetisation measurements were carried out in a three-axis cryogenic rock magnetometer of 2G Enterprises, equipped with an in-line alternating field demagnetiser. Isothermal remanent magnetisations were imparted to samples of each unit in a 2G pulse magnetiser in fields up to 2.6T. Small one-inch cubes were cut from the oriented block samples for AMS measurements in a KLY-3S magnetic susceptibility meter.

4. Experimental results

Rock magnetic properties and grain size analysis of all the units had been investigated in detail before the palaeomagnetic examination started (Jordanova et al. 2007). In brief, magnetic mineralogy deduced from thermomagnetic analysis of magnetic susceptibility, induced magnetisation in strong fields and Mössbauer analysis suggest that magnetite, oxidised magnetite and hematite are the main ferri- and antiferromagnetic phases present. Mössbauer analysis of magnetic separates from S_1 and L_2 yielded more or less similar results. The presence of maghemite was revealed in the strong magnetic fraction of S_1 but not in L_2. The clay content along the sequence does not vary significantly and the mean percentage, both in loess and soil horizons, is around 30. Exceptions are the less altered loess units L_2 and L_5 with lower clay content. The observed high clay content but small differences in clay content between soils and loesses are manifestation of the enhanced weathering and pedogenesis, even during the glacials, particularly in the lower part of the section. All the palaeosol units are characterised by high frequency dependent magnetic susceptibility (χ_{FD}%) with values up to 12%, pointing to a significant superparamagnetic (SP) fraction. A relatively high content of SP Fe_3O_4 grains can also be assumed for loess units L_1, L_3, L_6 and L_7 (Jordanova et al. 2007). The presence in loesses of pedogenic magnetically soft grains in the SP and viscous SP/SD (SD = single domain) state is also supported by the relatively low coercivity (B_c) and coercivity of remanence (B_{cr}) values in these units, comparable to the values attained in the palaeosols.

Additional rock magnetic experiments that are presented below yield further information about the nature and magnetic stability of the remanence carriers as well as of the magnetic fabric of all the units.

Fifteen samples were prepared from loose materials collected in all the units for a viscous remanent magnetisation (VRM) acquisition experiment. Mechanical redistribution of the grains, randomising any pre-existing remanence was chosen as a “demagnetisation”

technique. This option was preferred in order not to change the original domain state as is the case during AF demagnetisation (Jordanova et al. 2007), or mineralogy that often happens when heating loess and soil samples above their Curie-temperatures (Tc) followed by cooling in zero field. Gently crushed and sieved material was pressed into PVC cylinders and sealed with epoxy resin. Spontaneous VRM build-up in an ambient field of 48 μT was monitored over 2 months (Fig. 2). Samples from the upper part of the sequence (S_0 - L_4) show two different linear segments in the VRM versus log(t) graphs, separated at the elapsed time of about 6 weeks [corresponding to log (t) = 5.57]. Both palaeosols and loesses (respectively S_0-S_3 and L_1-L_4) show this peculiarity in contrast to the units from the lower part of the section (S_4 – L_7, red clay). Calculation of viscous acquisition coefficients (Sa), taking separately the two slopes of the VRM(log t) relationship (respectively Sa1 and Sa2), reveals the presence of a fraction that acquires viscous magnetisation more slowly. In order to evaluate the significance of an ultrafine grained fraction in the total viscosity, a plot of the Sa1 coefficients as function of χ_{FD}% (Forster et al., 1994) is given in Fig. 3. The leading role of the concentration on the amount of viscous acquisition is revealed by the good linear correlation between Sa1 and χ_{FD}% (with correlation factor $R^2 = 0.91$).

Stepwise IRM acquisition in pulse fields up to 2.6 T was monitored for 15 samples representative for each lithological unit. Magnetic mineral components contributing to the total remanence were unmixed, following the procedure by Heslop et al. (2002) and applying the IRM Unmix software. The initial state of the samples was an AF-demagnetisation state, which is most suitable when fitting log-normal distributions to IRM acquisition curves (Heslop et al., 2004). The best fit was obtained with a 3-component model and some representative examples are shown in Figure 4. Component 1, which is the main component in the palaeosol samples, is characterised by a relatively low coercivity maximum $B_{1/2}$ at around 27mT in the palaeosol as well as in the loess samples (Fig.4 and Table 1). In the

palaeosol samples it contributes from 40 up to 70% (with an average of 51%) to the total IRM. On the other hand, component 2 is the main component in the loess samples with an average contribution of 53% to the total IRM and a coercivity peak around 70 to 80mT. A distinct high-coercivity component, component 3, with quite varying maximum coercivities between about 150 and 960mT can be identified in all samples (Table 1 and Table 2). In general, maximum coercivities of component 3 are lower in palaeosol samples and most weathered loess samples compared to less weathered loesses. Irrespective of the nature of the samples it contributes around 13% to the total IRM (Table 1). A good linear correlation is observed between the absolute intensity of component 1 and the viscous acquisition coefficient Sa and/or Sa2 (for two-slope curves) (Fig. 5). From the $B_{1/2}$ versus relative contribution graph in Figure 6 and from Table 2 it is clear that the higher the coercivity of component 3, the smaller its relative contribution to the total IRM. Component unmixing for the sample from the recent soil S_0 reveals quite different values for the unmix parameters compared to the palaeosols and this is the reason to enter the data separately in Table 1.

Stepwise alternating field and thermal demagnetisations of IRM(2.6T) were applied to several samples in order to gain information about the unblocking spectra of the remanence carriers. The examples given in Figure 7 show a more or less similar behaviour for both loess and palaeosol samples. Median destructive fields (MDF) of IRM(2.6T) are in the range of 15.8 - 16.9mT for palaeosols and in the range 17.5 - 21.2mT for loesses (Fig. 7a). This very soft magnetic behaviour is accompanied by relatively high unblocking temperatures as can be seen from the thermal demagnetisation curves (Fig. 7b). Half of the total IRM is demagnetised between 270 and 300°C with a fairly continuous unblocking spectrum up to 680^{o}C, above which complete demagnetization of the initial IRM is observed. The slightly enhanced unblocking of IRM at about 300^{o}C, especially in the palaeosol samples, is

224 accompanied by a strong increase at the same temperature in the room-temperature magnetic
225 susceptibility measured after each heating-cooling step (Fig. 7c).

226 Anisotropy of magnetic susceptibility measurements on oriented one-inch cubes, cut
227 from the oriented block samples, reveal a normal sedimentary fabric with average maximum
228 (Kmax) and intermediate (Kint) susceptibility directions in the bedding plane (Fig. 8). The
229 scatter of principal directions is relatively high compared to other loess deposits (Matasova et
230 al., 2001; Hus, 2003; Lagroix and Banerjee, 2004; Zhu et al., 2004) but similar to the loess-
231 palaeosol sequence of Roxolany in Ukraine (Hus, 2003). Only the principal susceptibility
232 directions of specimens from the least weathered loess unit L2 are much less scattered (Fig.
233 8b). Table 3 summarizes the average principal anisotropy parameters lineation (L), foliation
234 (F), corrected degree of anisotropy (P´) and shape parameter T (Jelinek, 1981) for palaeosols,
235 loesses and red clay samples, respectively. No highly significant differences among the values
236 for the three groups can be observed. The low degree of anisotropy, less than 4%, is typical
237 for loesses and palaeosols. A slightly higher degree of 7% is obtained for the red clays.

238 The best "cleaning" technique for the determination of the characteristic remanent
239 magnetisation (ChRM) was chosen after stepwise thermal as well as alternating field (AF)
240 demagnetisation test experiments on pilot samples. The AF demagnetisation with increasing
241 maximum amplitude up to 150 mT reveals the presence of a very soft remanence component
242 (Fig. 9). Values of the MDF of NRM (MDF_{NRM}) are in the range 7.0 - 12.0mT for loess and
243 soil samples, consistent with the presence of a significant VRM in both. Moreover, there is a
244 negative relationship between MDF_{NRM} values and the percent relative contribution of the
245 first component from the IRM unmixing (Fig. 10). Figure 11 shows several examples of the
246 directional and intensity changes of loess and soil samples during stepwise thermal
247 demagnetisation. It is clear that besides a stable ChRM component; the samples contain an
248 important unstable component, probably of viscous origin. Cleaning temperatures of 300^{o}C,

325°C and 350°C were finally chosen to isolate the ChRM of the whole collection of oriented samples. The depth variation of the ChRM direction (declination D, inclination I) and intensity along the composite section after partial demagnetization at 325°C is given in figure 12a. The declination is predominantly eastward and attains relatively high values in the upper part of section 1 (S_1, L_2 and upper part of S_2), accompanied by relatively low inclination values. One single sample in the upper part of S_1 reaches an anomalous intermediate declination value. Below S_2, the profile declination varies around zero, but remains predominantly eastward down to loess unit L_7 (Fig. 12a), where it becomes southward accompanied by negative inclinations. This polarity change is interpreted as corresponding to the Matuyama/Brunhes transition. Higher resolution of the directional changes in L_7 was obtained in a parallel section (Fig.12b). The switching of the inclination is observed within the bottom part of loess unit L_7, where the loess becomes yellowish with large brown reddish veins suggesting strong leaching. Declination does not show any systematic behaviour and remains eastward when inclination becomes negative. Two reversed magnetozones can be recognized in the red clay unit, although in a few samples no stable end-direction could be reached after cleaning at 325°C. Rapid oscillations of declination within the upper part of the red clays (between 22 and 24m depth) complicate the interpretation of the geomagnetic field behaviour in this part of the record. The ChRM signal of a parallel section in the upper part of section 1, sampled at 5 cm interval, did not reveal any indication of short term field reversals or "excursions" similar to the Blake event (data not shown). Wiegank (1977) claimed to have found the latter in unit L_3 of a loess/palaeosol section near Russe on terrace T_6 of the Danube river.

5. Discussion

5.1. Remanence carriers and magnetic stability

According to the results from previous detailed rock magnetic investigations, magnetite and oxidised magnetites (maghemite) are the main remanence carriers in the palaeosol/loess units of the Viatovo sequence. (Jordanova et al. 2007). Viscous acquisition experiments reported this time contribute to a better understanding of their grain size distribution. The observed two-slope VRM acquisition in samples from the upper units (S_0, L_1, S_1, L_2, S_2, L_3, S_3, L_4) and single-slope in the older units (Fig. 2), probably indicates different populations of viscous grains in the upper part compared to the lower part of the sequence. This is consistent with the differentiation of palaeosol units according to the calculated background susceptibility for each unit in Jordanova et al. (2007). Previous studies by Evlogiev (2006) indicate that the recent soil S_0 and the first three palaeosols are Chernozems, while the older palaeosols show features of forest soils that developed in a more humid climate. Thus, it can be inferred that the soil type (e.g. climate) is the main factor determining magnetic grain size distribution of the pedogenically produced fine grained ferrimagnetic fraction. A possible explanation for the single-slope behaviour is that in the older palaeosols a higher degree of grain surface low-temperature oxidation has led to a more uniform population of viscous maghemite grains. On the other hand, in the dryer conditions of steppe vegetation, when Chernozems are formed, grains are expected still to have a non-oxidised core with oxidised rim. Such grains, in which the two phases are exchange coupled, are responsible for increased bulk coercivity (Van Velzen and Zijderveld, 1995; Cui et al., 1994; Dunlop and Ozdemir, 1997). The good correlation between χ_{FD}% and Sa coefficients, with R^2= 0.91, suggests that the concentration of fine viscous SP/SD grains is proportional to the degree of pedogenic enhancement both in palaeosol and loess units (Fig. 3). The dominant role of the fine grained fraction in the determination of magnetic viscosity of the loess/palaeosol samples is revealed by this linear relationship. This implies also that the “in situ” formed pedogenic fraction has a broad grain size distribution, spanning the whole range from SP, viscous SP/SD to stable SD grains.

Analysis and modelling of IRM acquisition curves by a set of log-normal probability density functions, applying an expectation – maximization algorithm and the IRMunmix program by Heslop et al. (2002), confirms the above conclusion. The results suggest that the best fit of the experimental data is obtained with a 3-component model (Fig. 4). Component 1 with $B_{1/2}$ of 27 (±3)mT on average and dispersion parameter DP of 0.24 (±0.02) is identified in both loess and palaeosol samples. It only varies in its relative contribution to the total IRM, with a maximum contribution in the palaeosols and a minimum in the loess samples (Table 1). Similar results have been reported by Spassov et al. (2003a) for the P-component in loess-palaeosol samples from the Lingtai section on the central Loess Plateau of China with $B_{1/2}$ of 31 (±4)mT. The second component yields a $B_{1/2}$ value of 35 (±8)mT or a slightly lower coercivity compared to the second component of Eyre (1996). The aforementioned data, as well as our data, are slightly higher than the reported $B_{1/2}$ value of 20mT and DP of 0.25 to 0.38 by Geiss and Zanner (2006) for the pedogenic component in modern loessic soils from mid-western United States. However, these authors analysed AF-demagnetisation curves of IRM, which yield systematically lower estimations of the bulk coercivity, because the mean interaction field in a sample is a demagnetising field that aids in AF demagnetisation but opposes IRM acquisition (Dunlop and Ozdemir, 1997). On the other hand, we obtained a good linear correlation between the estimated intensity of component 1 and the viscous acquisition coefficients Sa (for single – slope samples) and Sa2 (for two-slope samples) (Fig. 5). It confirms our view that the population of grains above the critical SP/SD size, which acquires an isothermal remanence, is a continuation of a common distribution of the pedogenic fraction.

Component 2 is characterized by $B_{1/2}$ of 70 (±12)mT and DP of 0.32 (±0.02) (Table 1). Its relative contribution is highest in the loess samples with values up to 59% and most probably corresponds to the presence of oxidised detrital magnetites.

Interpretation of the third component of the IRM unmixing should take into account the high variability of the coercivity $B_{1/2}$, which is in close relation to the degree of secondary alteration (Table 2). Moreover, the negative linear relationship of $B_{1/2}$ and the relative contribution of component 3 in Figure 6 strongly suggest that this component represents detrital SD-PSD grains with progressively higher degree of low-temperature oxidation of magnetite to maghemite and, finally, hematite. But the observed very soft magnetic behaviour of IRM against AF-demagnetisation (Fig. 7a) suggests that hematite does not contribute significantly to the total remanence.

The enhanced unblocking of the isothermal remanence at around 300°C in Figure 7b can be interpreted as being related to the inversion of maghemite (Evans and Heller, 1994). This interpretation is supported by the obtained mean coercivity of the first component of the IRM acquisition, corresponding quite well to the reported values for SD magnetites (Maher, 1988) and maghemites (Enkin and Dunlop, 1987). At the same time, the strong increase in bulk magnetic susceptibility measured after each heating step (Fig. 6c) is probably ~~is~~ due to thermal transformation of the clay minerals and Fe-oxyhydroxides (lepidocrocite, ferrihydrite, goethite) in the presence of reducing agents (organic matter) (Cornell and Schwertmann, 1996; Campbell et al., 1997) and partly caused by remanence unblocking. Thermal demagnetisation of IRM(2.6T) (Fig. 7b) indicates also that there is still some remanence demagnetised at temperatures well beyond 620°C. Similar parameters and thermal behaviour have been observed for the detrital component D2 by Spassov et al. (2003a) and interpreted by these authors as being carried by altered detrital magnetites.

5.2. Palaeomagnetism: ChRM and magnetostratigraphy

348 The preservation of the original detrital fabric in weakly consolidated sediments, like loess
349 and palaesols,is some guarantee in magnetostratigraphical investigations that the directional
350 results are not entirely influenced by secondary alterations and mechanical disturbances. AMS
351 measurements of all the units of the Viatovo section (Fig. 8a) show that despite some high
352 scatter in the distribution of the principal susceptibility directions, a typical depositional
353 magnetic fabric is still preserved with Kmax on average in the horizontal (bedding) plane and
354 Kmin in the vertical plane. Shallower inclination values of Kmin for several samples are
355 obviously due to bioturbation and may be also to clay films (translocation) along vertical
356 cracks as it could be observed in the field. As shown in previous studies (Hus, 2003), "in situ"
357 formation of the pedogenic magnetic fraction does not influence very much the primary
358 magnetic fabric of loess sediments. The better grouping of the Kmin directions for samples
359 from unit L_2 (Fig. 8b), the loess unit least affected by secondary alterations and bioturbation,
360 confirms our assumption that mechanical disturbance due to bioturbation in the other units is
361 the main cause for the scatter in the principal directions. The low degree of anisotropy and
362 foliation (Table 3) indicate that the magnetic fabric, governed mainly by the ferrimagnetic
363 fraction because of relatively high mean susceptibility values, is quite isotropic.
364 Alternating field demagnetisation of NRM revealed very soft behaviour (Fig. 9) with less
365 than 20% of the original signal left after treatment in a 30mT field. This prevailing
366 contribution of the low-coercivity component (probably responsible for the VRM) led us to
367 choose thermal treatment as the optimal technique for determining the characteristic
368 remanence direction. Furthermore, the observed correlation between MDF_{NRM} and the relative
369 contribution of component 1 (identified by the IRM unmixing procedure in Figure 10 and
370 interpreted as pedogenic maghemite) convinced us that AF cleaning would be less successful
371 in isolating the characteristic remanence carried by the detrital magnetites (component 2) and
372 magnetites oxidised at different degree (component 3).

Stepwise thermal demagnetisation experiments revealed the presence of a secondary component more or less in the present day magnetic field direction (Fig. 11), probably of viscous or chemical origin. This component is demagnetised upon heating to 200 – 250^{o}C, which is also indicated by the change in slope of the NRM intensity versus temperature curves. ChRM directions after partial demagnetisation at 300, 325 and 350°C were determined by principal component analysis and show consistent behaviour (Fig. 12). Some scattered directions and the two normal directions at the M/B polarity reversal interval may be due some mechanical disturbance of the loess material and chemical overprinting after deposition as suggested by the presence of large secondary carbonate concretions and clayey reddish veins (see also Zhu et al., 2006). Another reason for the observed rapid directional changes during polarity transitions may be the lock-in depth mechanism in loess-palaeosol sediments and/or chemical overprinting as described in Spassov et al. (2003b). An earlier palaeomagnetic investigation of the lower part of the loess complex near Russe, in the Nikolovo section, located the M/B boundary between units S_6 and L_7 (Butchvarova, 1993). The magnetisation of the red clay unit switches twice from reversed to normal polarity (Fig. 12). According to the results of the rock magnetic investigations (Jordanova et al, 2007), the red clay unit may be considered as a thick pedocomplex that formed in subaerial conditions with high weathering potential. Magnetic susceptibility variations suggest the presence of at least two palaeosols (Fig. 12). The two periods of normal polarity correspond with an increase in magnetic susceptibility in the two sub-units. The normal polarity magnetozone revealed in the upper part of the red clay unit is assumed to correspond to the Jaramillo subchronozone (0.99 - 1.07 Ma) or spanning stages 27 to 31 of the δ^{18}O chronology (Shackleton et al., 1990; Tiedemann et al., 1994). The second normal polarity event is found in the middle of the red clays. Because of its relatively long duration and the lower age estimate of the red clay complex at 2.6 Ma (Evlogiev, 1993) it can be reasonably assumed that it corresponds to the

Olduvai subchron (1.78 - 1.94 Ma). Indeed, the short lived Cobb Mountain event identified in deep-sea sediments (Biswas et al., 1999; Yang et al., 2004) is unlikely to have been recorded or preserved in the record because of a low sedimentation rate, smoothing and post-depositional alterations. Indeed, this event is rarely found in loess/soil sequences (Rolph et al., 1989). The recently reported Kamikatsura and Santa Rosa short-lived geomagnetic excursions in loess unit L_9 of the Chinese loess (Yang et al., 2004) are probably absent in the Viatovo section for the same reasons – the low sedimentation rate as well as the strong secondary alteration of loess unit L_7. The absence of the Blake event in the Viatovo section is not unusual, as discussed in other studies (Zhu et al., 1998; Stevens et al., 2006). Its presence would have been of great importance for the Late-Pleistocene stratigraphy of the loess/palaeosol sequence and for the identification of the last interglacial palaeosol. Indeed, in many loess deposits in Western Europe (Hus and Geeraerts, 1986) the first palaeosol encountered in depth is not an interglacial but an interstadial soil corresponding to stage 3 of the oxygen isotope record (Shackleton et al., 1990). Therefore, the stratigraphy of the upper part of the Viatovo sequence is deduced by correlation of its magnetic susceptibility signature with the astronomically tuned δ^{18} O record from ODP site 677 (Fig. 13). According to the previous established correlation between the magnetic susceptibility record of a core taken in the loess/palaeosol sequence in Koriten in NE Bulgaria (Jordanova and Petersen, 1999), palaeosol S_1 in Viatovo is the last interglacial (Eemian) soil (Fig. 13). Stage 3 is witnessed in Viatovo by some high magnetic susceptibility values in the upper part of L_1, similar to the Koriten record. With the two time constraints in the sequence, the Eemian soil and the position of the M/B boundary, the one to one correspondence between magnetic susceptibility variations and the δ^{18}O variations in the ODP 677 record strongly suggests that each palaeosol that can be recognised in the Viatovo sequence corresponds to an interglacial.

6. Conclusions:

1. Magnetic mineralogy (nature and magnetic domain state) of the loess-palaeosol units from the Viatovo section deduced from unmixing IRM acquisition curves, VRM acquisition experiments and thermal demagnetization of IRM(2.6T) indicate the presence of pedogenic magnetite/maghemite particles spanning SP, viscous SP/SD and stable SD sizes. Their contribution is especially enhanced in the palaeosols. Detrital magnetic minerals are probably oxidised PSD magnetites, whereas the contribution of hematite to the magnetic properties is insignificant. A three component model fits best the experimental IRM acquisition curves. The third component shows highly variable mean magnetic coercivity among the samples, reflecting the degree of alteration of the original detrital magnetite grains with increasing oxidation.
2. The magnetic fabric of loess/palaeosol samples from the Viatovo section, revealed by AMS measurements, points to an initial normal sedimentary fabric that has been modified to some degree after deposition by pedogenic processes. Field evidence shows that the scatter of the principal susceptibility directions can be mainly attributed to mechanical disturbances due to bioturbation (presence of crotovinas) and eventually clay migration along cracks.
3. The record of the Matuyama – Brunhes polarity transition in loess unit L_7 displays several rapid directional changes of the characteristic remanence.
4. Notwithstanding strong pedogenesis, weathering and viscous overprints, a detailed magnetostratigraphy of the Viatovo section in North Bulgaria could be established. The Matuyama/Brunhes boundary has been recorded in the oldest loess unit L_7 present. Two normal polarity magnetozones, discovered in the underlying red clay formation, probably correspond to the Jaramillo and Olduvai subchronozones.

Acknowledgements. This research benefited from a bi-lateral cooperation grant between the Geophysical Institute of the Bulgarian Academy of Sciences and the Geophysical Centre of the Royal Meteorological Institute of Belgium (project 1-12).

References:

Biswas, D., Hyodo, M., Taniguchi, Y., Kaneko, M., Katoh, S., Sato, H., Kinugasa, Y., Mizuno, K., 1999. Magnetostratigraphy of Plio-Pleistocene sediments in a 1700-m core from Osaka Bay, southwestern Japan and short geomagnetic events in the middle Matuyama and early Brunhes chrons. Paleogeogr., Paleoclimatol., Paleoecol., 148, 233-248.

Butchvarova,V., 1993. Magnetostratigraphy of Neogene - Quaternary sediments from Eastern and Central Parathetys. Ph. D. Thesis, Bulgarian Academy of Sciences, Sofia (in Bulgarian).

Campbell, A., Schwertmann, U., Campbell, P., 1997. Formation of cubic phases on heating ferrihydrite. Clay Minerals, 32, 615-622.

Cornell, R. and Schwertmann, U., 1996. The Iron Oxides. Structure, properties, reactions, occurrence and uses. VCH Verlagsgesellschaft, Weinheim, New York.

Cui, Y., Verosub, K., Roberts, A., 1994. The effect of low temperature oxidation on large multidomain magnetite. Geophys. Res. Lett., 21, 757 – 760.

Dodonov, A., Zhou, L.P., Markova, A., Tchepaliga, A., Trubikhin, V., Aleksandrovski, A., Simakova, A., 2006. Middle-Upper Pleistocene bio-climatic and magnetic records of the Northern Black Sea Coastal Area. Quat. Int., 149, 44-54.

472 Dunlop, D. and Ozdemir, O., 1997. Rock Magnetism. Fundamentals and frontiers, (D.
473 Edwards, ed.), Cambridge Studies in Magnetism, Cambridge University Press.
474 Enkin, R., Dunlop, D., 1987. A micromagnetic study of pseudo-single-domain remanence in
475 magnetite. J. Geophys. Res., 92, 12 726 – 12 740.
476 Evans, M. and Heller, F., 1994. Magnetic enhancement and palaeoclimate: study of a
477 loess/palaeosol couplet across the Loess Plateau of China. Geophys. J. Int., 117, 257-
478 264.
479 Evlogiev, J., 1993. Palaeogeography and stratigraphy of the Early Pleistocene in near Danube
480 Northeastern Bulgaria. Ph.D. Thesis, Bulgarian Academy of Sciences, Sofia, (in
481 Bulgarian).
482 Evlogiev, J., 2006. The Pleistocene and Holocene in the Danube plain. Doctoral Dissertation
483 Bulg. Acad. Sci., Sofia. (in Bulgarian).
484 Eyre, J., 1996. The application of high resolution IRM acquisition to the discrimination of
485 remanence carriers in Chinese loess. Studia geoph. et geod., 40, 234 – 242.
486 Forman, S. L., Pierson, J., Lopper, K., 2000. Luminescence Geochronology. . In: Quaternary
487 Geochronology. Methods and Applications. AGU Reference Sheet 4, eds: J. Noller, J.
488 Sowers, W. Lettis Washington, DC, 157 – 176.
489 Forster, T., M. Evans and F. Heller, 1994. The frequency dependence of low field
490 susceptibility in loess sediments. Geophys. J. Int., 118, 636-642.
491 Geiss, C. E. and Zanner, C.W., 2006. How abundant is pedogenic magnetite? Abundance and
492 grain size estimates for loessic soils based on rock magnetic analyses. J. Geophys.
493 Res., 111, B12S21, doi: 10.1029/2006JB004564.
494 Gendler, T., Heller, F., Tsatskin, A., Spassov, S., du Pasquier, J., Faustov, S., 2006.
495 Roxolany and Novaya Etuliya – key sections in the western Black Sea loess area:

Magnetostratigraphy, rock magnetism, and paleopedology. Quat. Int., 152 – 153, 89 – 104.

Heslop, D., Dekkers, M., Kruiver, P., van Oorschot, H., 2002. Analysis of isothermal remanent magnetization acquisition curves using the expectation – maximization algorithm. Geophys. J. Int., 148, 58 – 64.

Heslop, D., McIntosh, G., Dekkers, M., 2004. Using time- and temperature-dependent Preisach models to investigate the limitations of modelling isothermal remanent magnetization acquisition curves with cumulative log Gaussian functions. Geophys. J. Int., 157, 55 – 63.

Huntley, D., Godfrey-Smith, D., Thewalt, M., 1985. Optical dating of sediments. Nature, 313, 105 – 107.

Hus, J., and Geeraerts, R., 1986. Palaeomagnetic and rock-magnetic investigation of Late-Pleistocene loess deposits in Belgium. Phys. Earth Planet. Inter., 44, 21-40.

Hus, J., 2003. The magnetic fabric of some loess/palaesol deposits. Phys. Chem. Earth, 28, 689-699.

Hutt, G., Jaek, I., Tchonka, J., 1988. Optical dating: K-feldspars optical response stimulation spectra. Quat. Sci. Rev., 7, 381 – 385.

Jelinek V., 1981. Characterization of the magnetic fabric of rocks. Tectonophysics, 79, 63-67

Jordanova, D. and Petersen, N., 1999. Palaeoclimatic record from a loess-soil profile in northeast Bulgaria – II. Correlation with global climatic events during the Pleistocene. Geophys. J. Int.., 138**,** 2, 533-540.

Jordanova, D., Jordanova, N., Henry, B., Hus, J., Bascou, J., Funaki, M., Dimov, D., 2007. Changes in mean magnetic susceptibility and its anisotropy of rock samples as a result of alternating field demagnetization. Earth Planet. Sci. Lett., 255, 3-4, 390 – 401.

520 Jordanova, D., Hus, J. and Geeraerts, R., 2007. Palaeoclimatic implications of the magnetic
521 record from loess/palaeosol sequence Viatovo (NE Bulgaria). Geophys. J. Int., 171,
522 1036-1047. doi: 10.1111/j.1365-246X.2007.03576.x
523 Lagroix, F., Banerjee, S., 2004. The regional and temporal significance of primary Aeolian
524 magnetic fabrics preserved in Alaskan loess. Earth Planet. Sci. Lett., 225, 379 – 395.
525 Matasova, G., Petrovsky, E., Jordanova, N., Zykina, V., Kapicka, A., 2001. Magnetic study of
526 Late Pleistocene loess/palaeosol sections from Siberia: palaeoenvironmental
527 implications. Geophys. J. Int., 147 (2), 367 – 380.
528 Maher, B., 1988. Magnetic properties of some synthetic sub-micron magnetites. Geophys. J.,
529 94, 83 – 96.
530 Nawrocki, J., Bogucki, A., Lanczont, M., Nowaczyk, N., 2002. The Matuyama – Brunhes
531 boundary and the nature of magnetic remanence acquisition in the loess-palaeosol
532 sequence from the western part of the East European loess province. Palaeogeogr.
533 Palaeoclimatol. Palaeoecol., 188, 39 – 50.
534 Pye, K., 1987. Aeolian dust and dust deposits. Academic Press, Harcourt Brace Jovanovich
535 Publ., London.
536 Rolph, T., Shaw, J., Derbyshire, E. and Wang, J.T., 1989. A detailed geomagnetic record
537 from Chinese loess. Phys. Earth Planet. Inter. 56, 151-164.
538 Shackleton, N., Berger, A. and Peltier, R., 1990. An alternative astronomical calibration of the
539 lower Pleistocene timescale based on ODP site 677. Trans. Royal Soc. Edinburg Earth
540 Sciences, 81, 251-261.
541 Singhvi, A.K., Bluszcz, A., Bateman, M.D., Someshwar Rao, M., 2001. Luminiscence daing
542 of loess-palaeosol sequences and coversands: methodological aspects and
543 palaeoclimatic implications. Earth Sci. Rev., 54, 193 – 211.

544 Spassov, S., Heller, F., Kretzchmar, R., Evans, M., Yue, L., Nourgaliev, D., 2003a. Detrital
545 and pedogenic magnetic mineral phases in the loess/palaeosol sequence at Lingtai,
546 (Central Chinese Loess Plateau). Phys. Earth Planet. Inter., 140, 255 – 275.
547 Spassov, S., Heller, F., Evans, M., Yue, L., von Dobenek, T., 2003b. A lock-in model for the
548 complex Matuyama-Brunhes boundary record of the loess/palaeosol sequence at
549 Lingtai (Central Loess Plateau). Geophys. J. Int., 155 (2), 350 – 366.
550 Stevens, Th., Armitage, S., Lu, H., Thomas, D., 2006. Sedimentation and diagenesis of
551 Chinese loess: Implications for the preservation of continuous, high-resolution climate
552 records. Geology, 34, 10, 849 – 852, doi: 10.1130/G22472.1
553 Tiedemann, R., Sarnthein, M., Shackleton, N., 1994. Astronomic timescale for the Pliocene
554 Atlantic $\delta^{18}O$ and dust flux records of Ocean Drilling Program site 659.
555 Paleoceanography, 9, 619-638.
556 Trumbore, S. E., 2000. Radiocarbon Geochronology. In: Quaternary Geochronology.
557 Methods and Applications. AGU Reference Sheet 4, eds: J. Noller, J. Sowers, W.
558 Lettis Washington, DC, 41 – 60.
559 Tsatskin, A., Heller, F., Gendler, T., Virina, E., Spassov, S., du Pasquier, J., Hus, J.,
560 Hailwood, E., Bagin, V. and Faustov, S., 2001. A new scheme of terrestrial
561 paleoclimate evolution during the last 1.5 Ma in the Western Black Sea region:
562 integration of soil and loess magnetism. Phys. Chem. Earth, Vol. 26, No. 11-12, 911-
563 916.
564 Van Velzen, A. and Zijderveld, J., 1995. Effects of weathering on single-domain magnetite in
565 Early Pliocene marine marls. Geophys. J. Int., 121, 267-278.
566 Wehmiller, J. F. and Miller, G. H., 2000. Aminostratigraphic Dating Methods in Quaternary
567 Geochronology. In: Quaternary Geochronology. Methods and Applications. AGU
568 Reference Sheet 4, eds: J. Noller, J. Sowers, W. Lettis Washington, DC, 187 – 223.

569 Wiegank, F., 1977. Untersuchungen zur palaomagnetischen Datierung von Losen und
570 Terrassen-sediment im Norden der Volksrepublik Bulgarien. Z. geol. Wiss., Berlin, 5**,**
571 3, 373-384.
572 Yang, T., Hyodo, M., Yang, Z., Fu, J., 2004. Evidence for the Kamikatsura and Santa Rosa
573 excursions recorded in eolian deposits from the southern Chinese Loess Plateau. J.
574 Geophys. Res., 109, B12105, doi: 10.1029/2004JB002966.
575 Zhu, R, Coe, R.S., Guo, B., Anderson, R. and Zhao, X., 1998. Inconsistent palaeomagnetic
576 recording of the Blake event in Chinese loess related to sedimentary environment.
577 Geophys. J. Int., 134, 867-875.
578 Zhu, R., Liu, Q., Jackson, M., 2004. Paleoenvironmental significance of the magnetic fabrics
579 in Chinese loess-palaeosols since the last interglacial (<130 ka). Earth Planet. Sci.
580 Lett., 221, 55 – 69.
581 Zhu, R., Liu, Q., Pan, Y., Deng, C., Sun, J., 2006. Identifying the origin of the magnetic
582 directional anomalies recorded in the Datong loess profile, northeastern Chinese loess
583 plateau. Geophys. J. Int., 164, 312 – 318.
584

585 **Figure and Table caption**

586

587 Fig. 1. a) Main geomorphological units in NE Bulgaria. Legend: 1- Holocene, Upper- and
588 Middle Pleistocene river and sea terraces; 2- Lower Pleistocene river- and marine
589 terrace T6; 3- Old Abrasive Accumulation Level (OAAL); 4- Pliocene Denudational
590 Surface (PDS); b) View of the loess-palaeosol section in the eastern part of the kaolin
591 quarry in Viatovo.

592 Fig. 2. VRM acquisition experiments for a) loess samples and b) palaeosol samples. Time t is
593 in seconds.

594 Fig. 3. Linear correlation between viscous acquisition coefficients Sa1 (calculated from the
595 first slope in two-slope curves and from all points for single-slope curves) and percent
596 frequency dependent magnetic susceptibility χfd%.

597 Fig. 4. Gradient acquisition plot (GAP) for representative samples from loess and palaeosols
598 fit with a 3-components model using expectation – maximization algorithm of Heslop
599 et al., 2002.

600 Fig. 5. Correlation between viscous acquisition coefficients Sa and the intensity of component
601 1 obtained from the IRM unmixing procedure. In case of two-slope curves, the slope
602 of the second linear segment Sa2 is taken and plotted as open diamonds. Full squares
603 denote Sa from single slope curves.

604 Fig. 6. Dependence of the relative contribution of each component with the corresponding
605 mean coercivity B1/2. Negative correlation is observed for component 3.

606 Fig. 7. Alternating field (a) and thermal (b) demagnetization of IRM(2.6T) of loess and
607 palaeosol samples and the behaviour of room-temperature bulk magnetic
608 susceptibility, measured after each heating step (c).

609 Fig. 8. Stereographic projections (on the lower hemisphere) of the maximum (Kmax) and
610 minimum (Kmin) susceptibility axes for loess and palaeosol samples from different
611 units (a) and b) principal susceptibility axes (Kmax, Kint, Kmin) for samples from
612 second loess unit L_2 only.
613 Fig. 9. NRM intensity changes during stepwise AF-demagnetization of loess and palaeosol
614 samples.
615 Fig. 10. Dependence between the MDF_{NRM} and the relative contribution of component 1,
616 obtained after unmixing IRM acquisition curves for the same specimens.
617 Fig. 11. Thermal demagnetization behaviour (direction and intensity) of representative
618 samples with normal and reversed ChRM directions.
619 Fig. 12. a) Depth variation of bulk magnetic susceptibility, declination, inclination and
620 intensity of the characteristic remanence ChRM (after thermal cleaning at 325^{o}C) in
621 the Viatovo section ; b) Declination, inclination and ChRM along unit L_7 in a parallel
622 section, sampled in more detail.
623 Fig. 13. Correlation of the magnetic susceptibility signatures of the loess/palaeosol sequences
624 in Koriten (Jordanova and Petersen, 1999) and Viatovo with the astronomically tuned
625 $\delta^{18}O$ changes in ODP 677.
626 Table 1. Mean values of parameters of the three components (log-normal Gaussian functions)
627 representing the best fit to experimental IRM acquisition curves for recent soil So,
628 loess units and palaeosols separately. Relative contribution of each component is given
629 in percent; B1/2 is the coercivity at which the gradient acquisition curve (GAP) is
630 centred; dispersion parameter DP is the width at half intensity of the GAP and
631 represents one standard deviation.
632 Table 2. Parameters of the third component obtained after fitting experimental IRM
633 acquisition curves for different samples.

634 Table 3. Mean values of principal anisotropy of magnetic susceptibility parameters for
635 loesses, palaeosols and the red clay unit. N is number of samples; standard deviations
636 of the mean values are given between brackets.
637
638

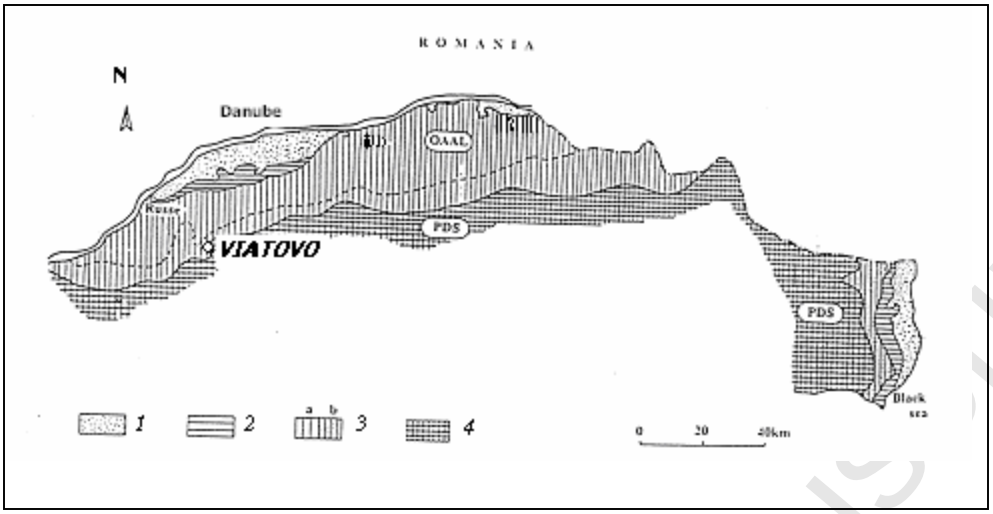

Figure 1

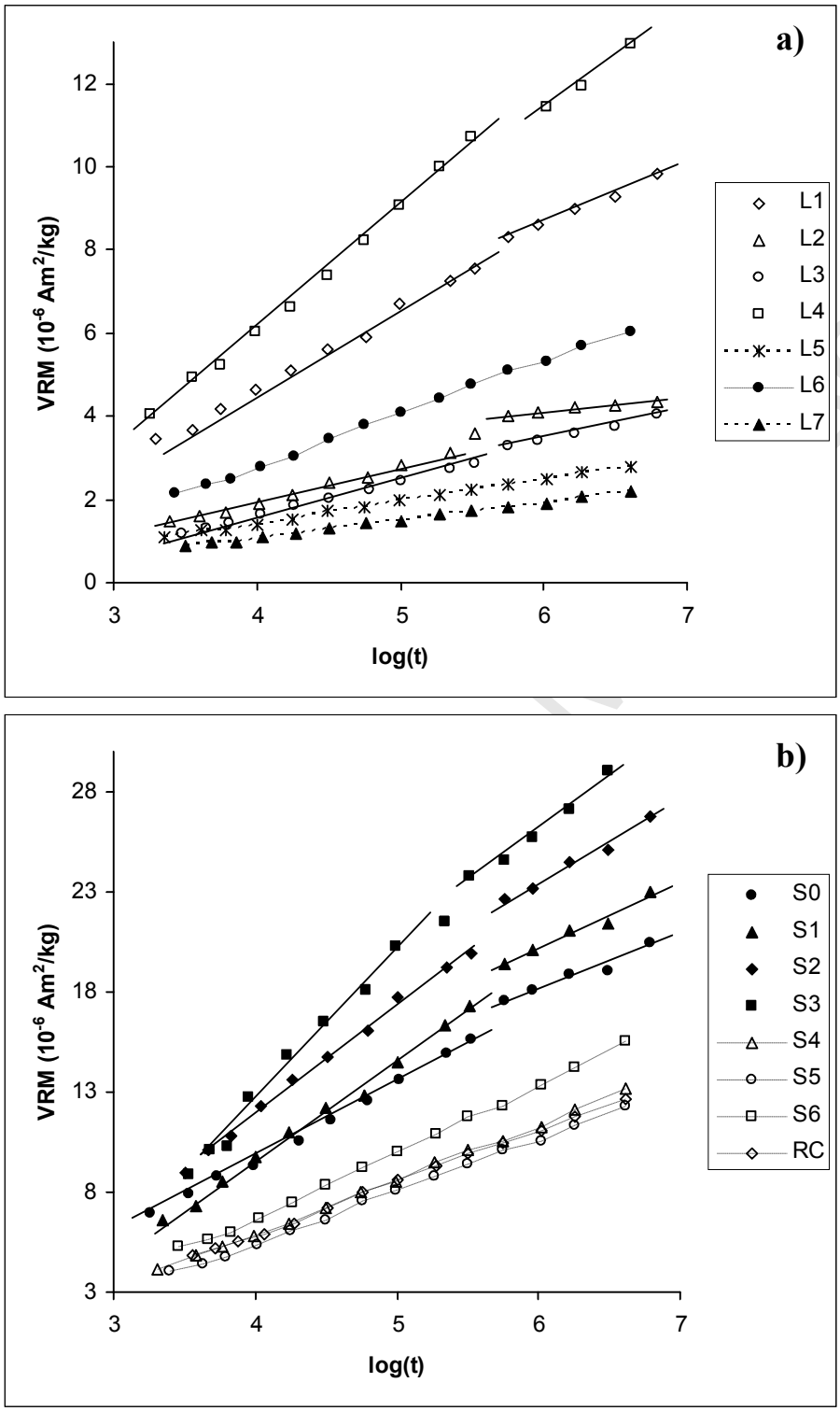

Figure 2

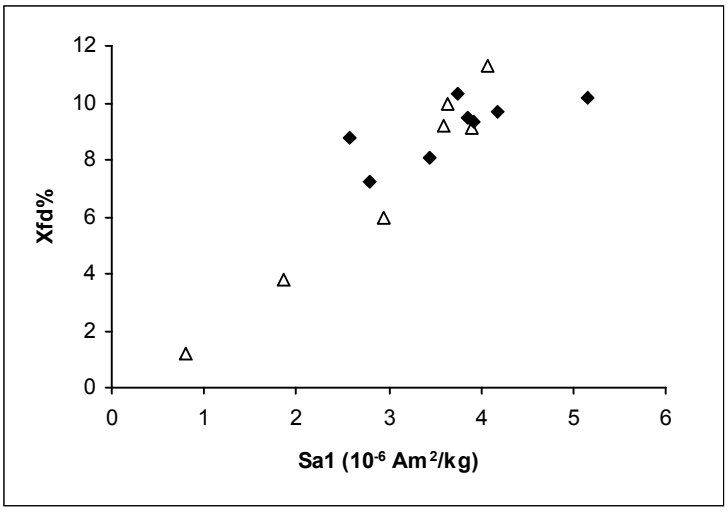

Figure 3

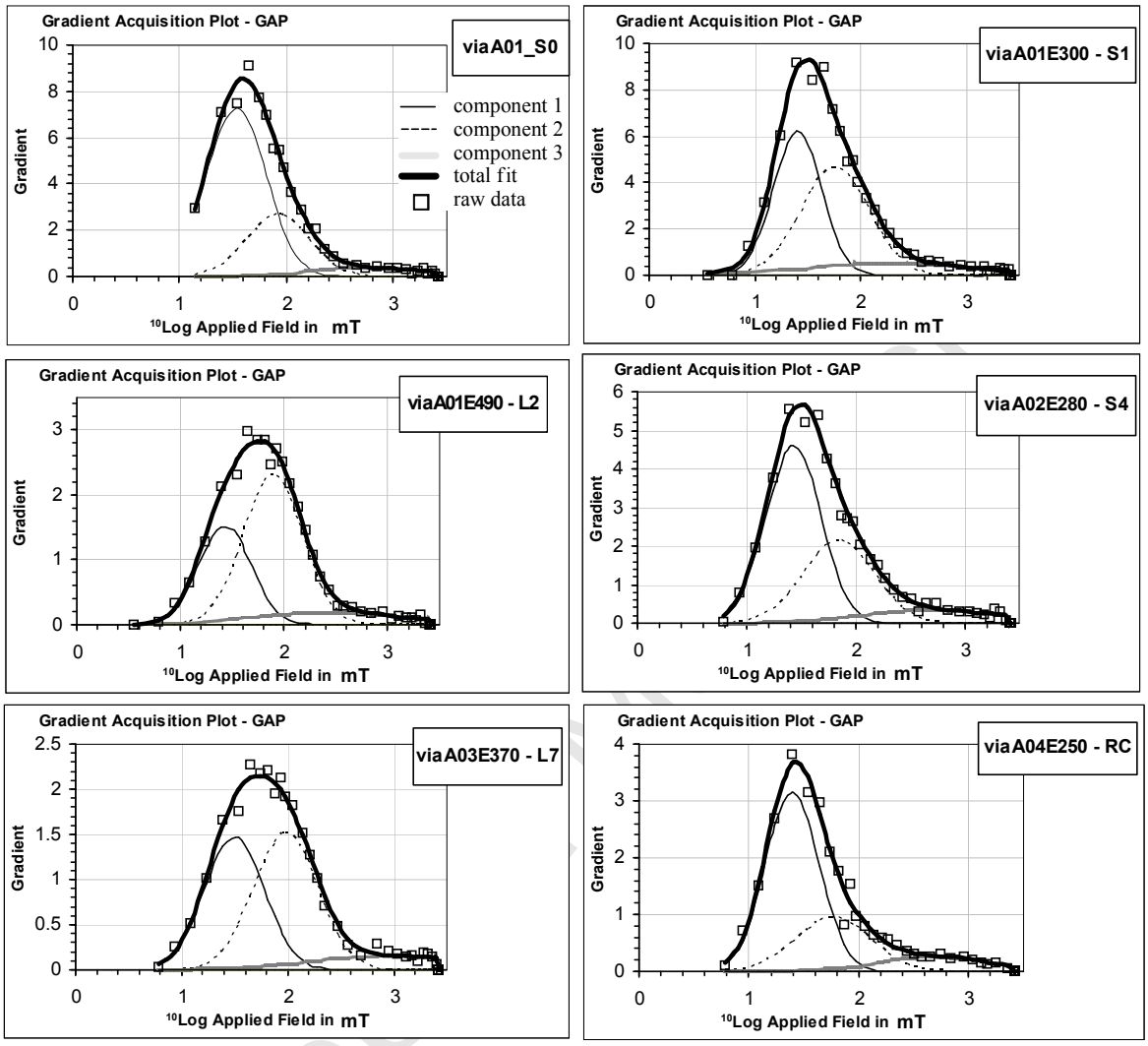

Figure 4

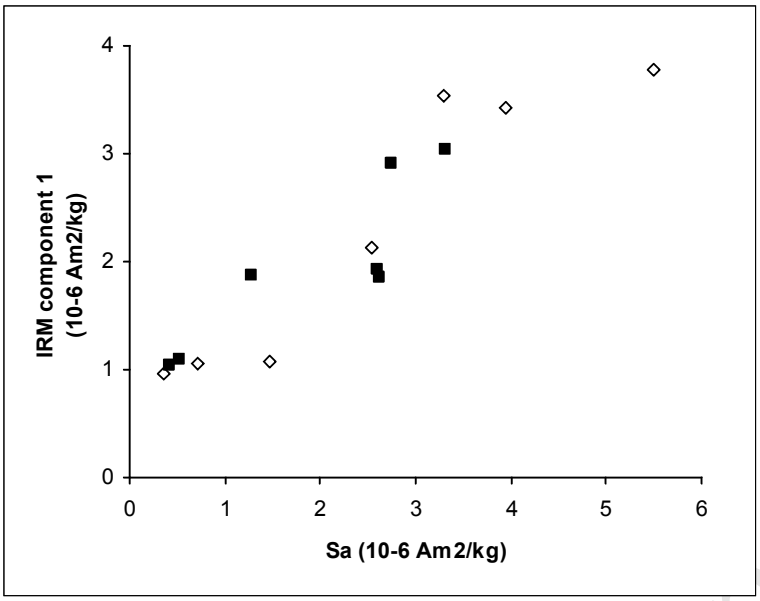

Figure 5

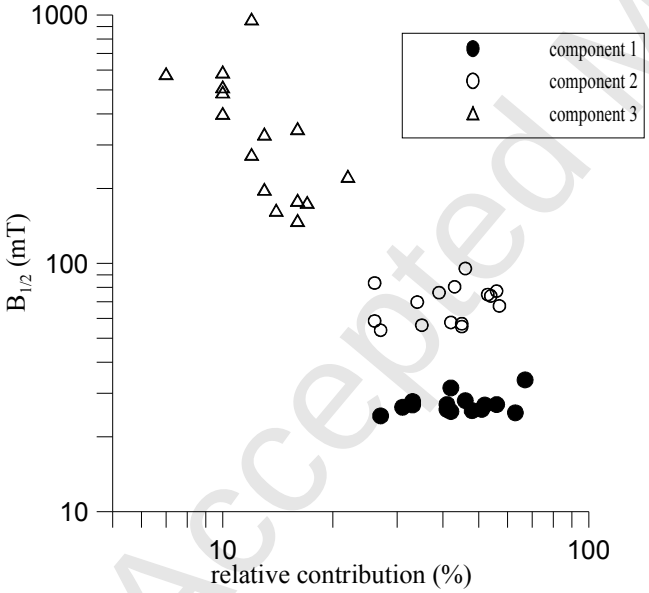

Figure 6

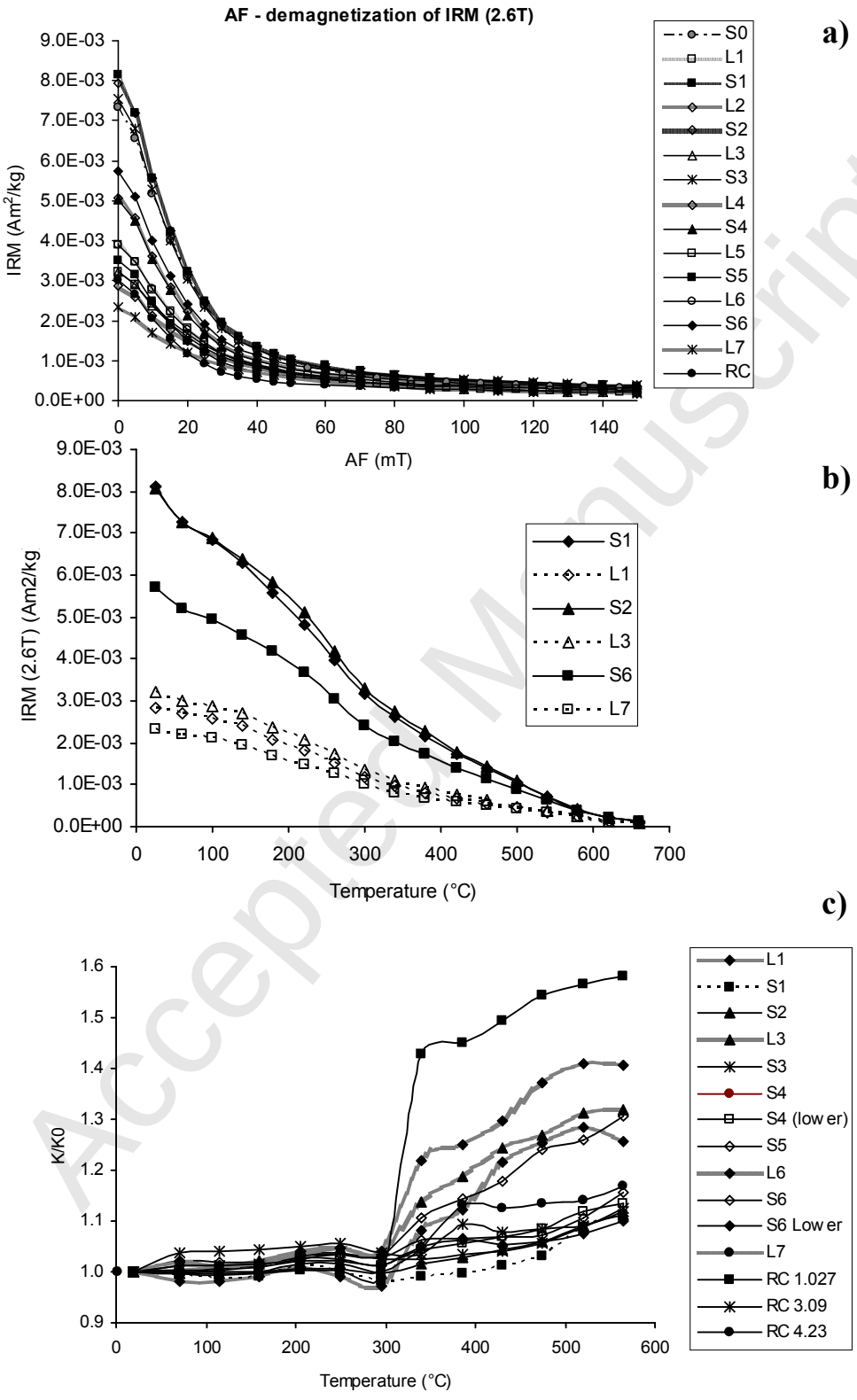

Figure 7

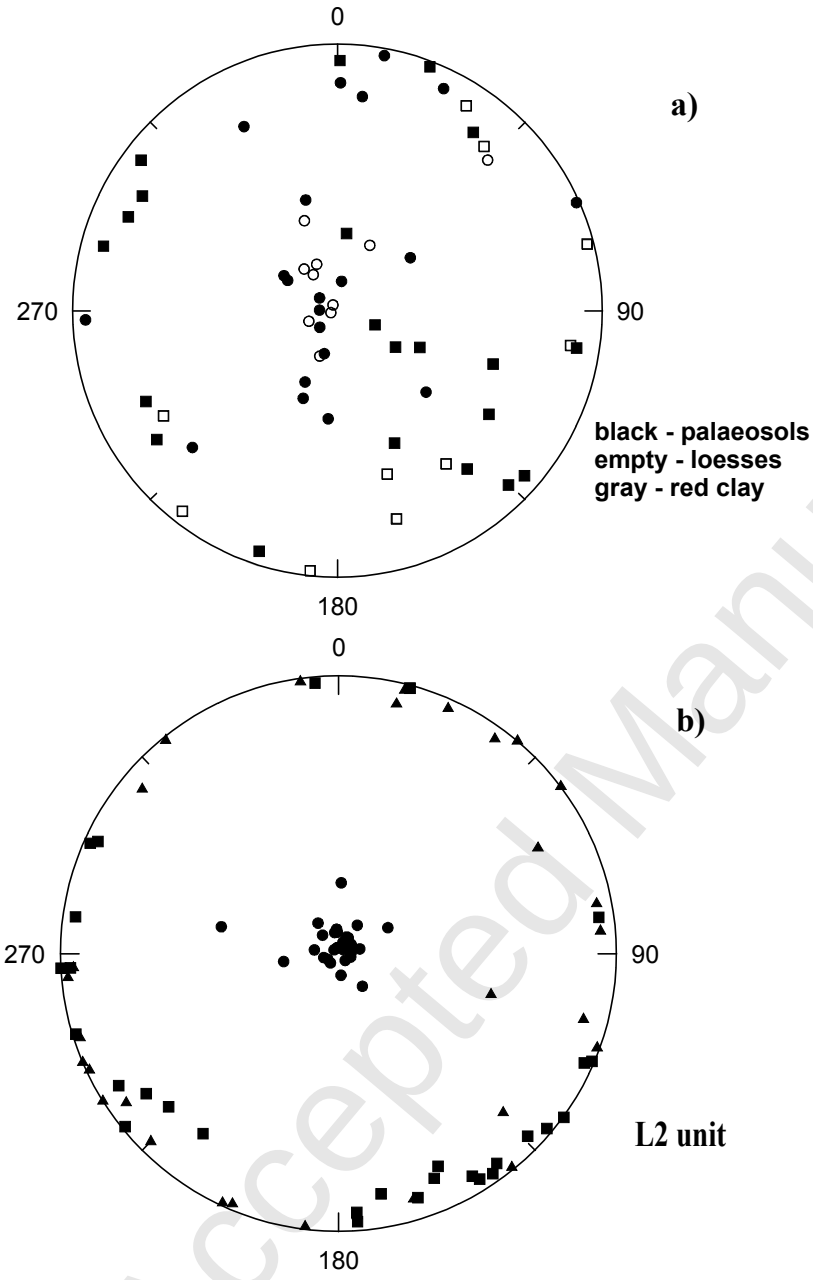

Figure 8

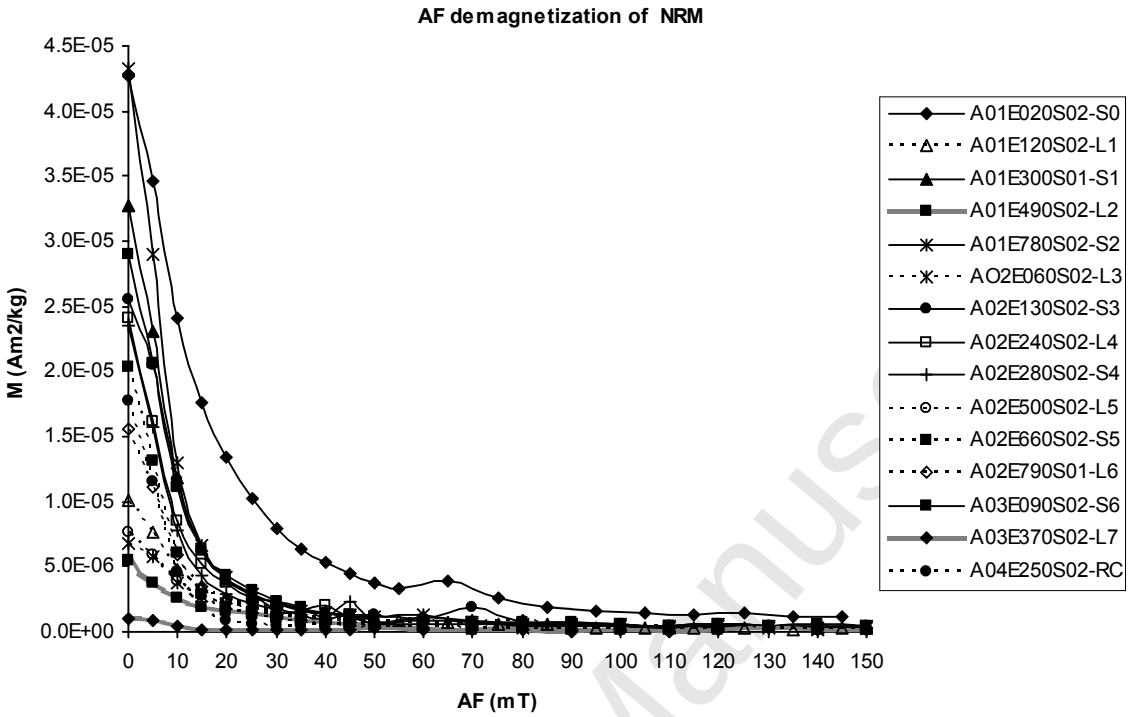

Figure 9

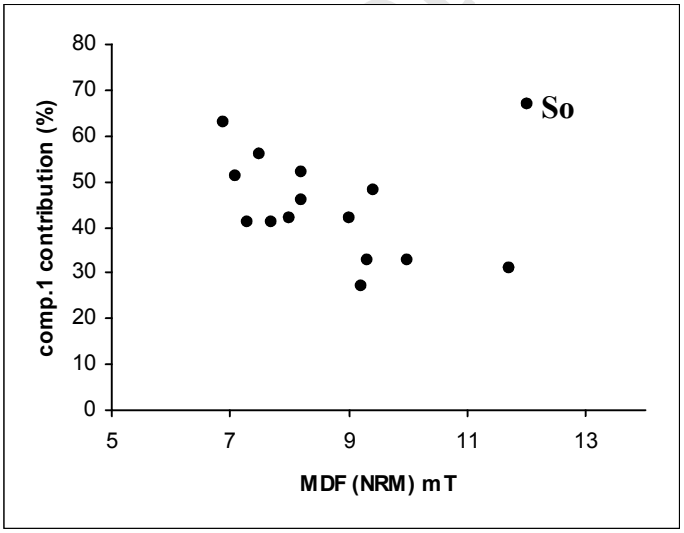

Figure 10

Figure 11

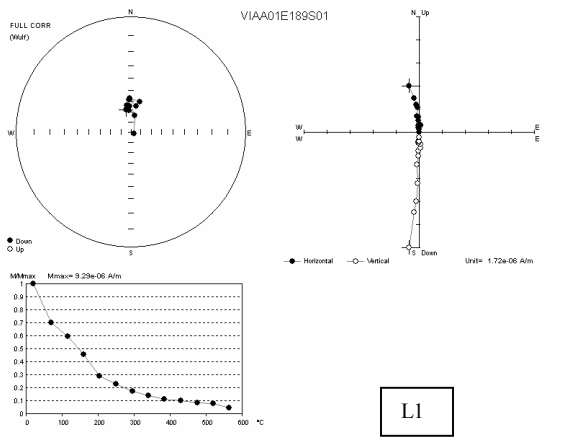

L1

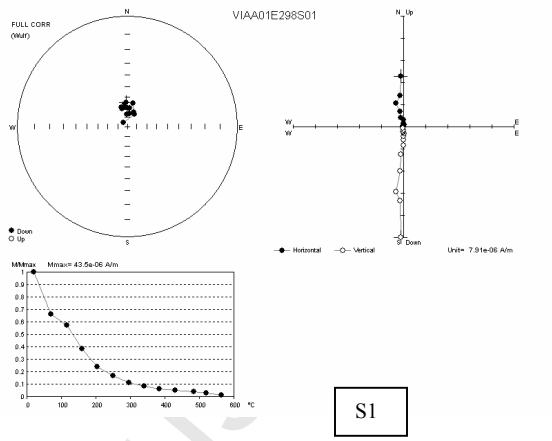

S1

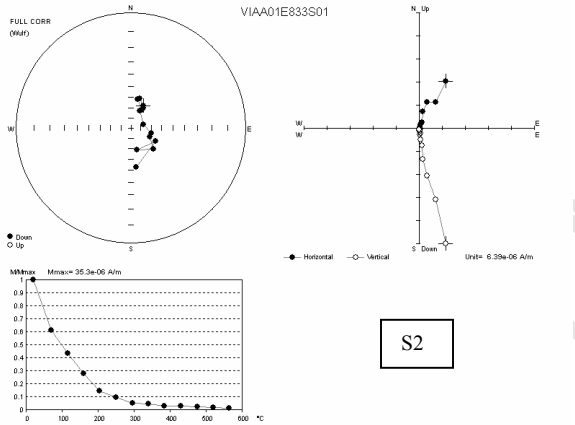

S2

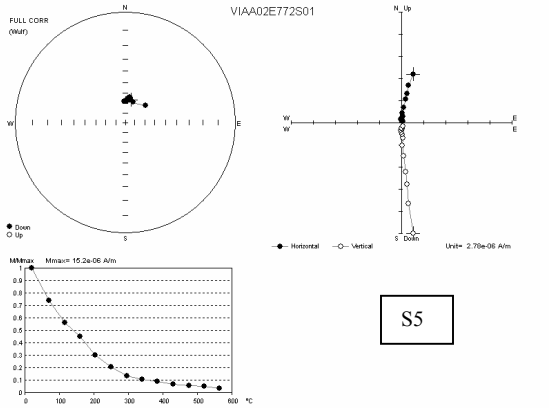

S5

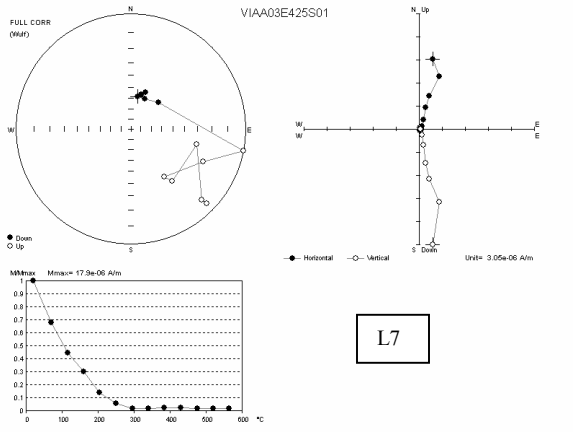

L7

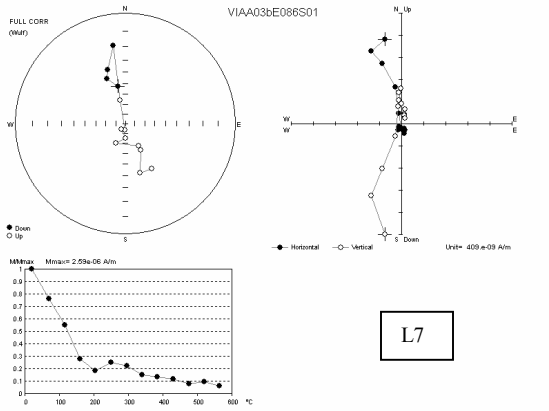

L7

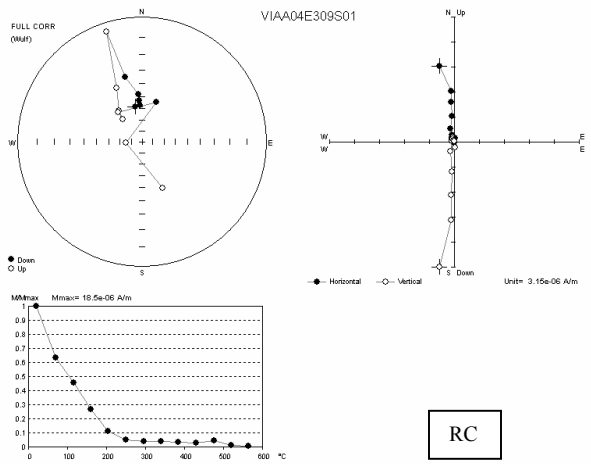

RC

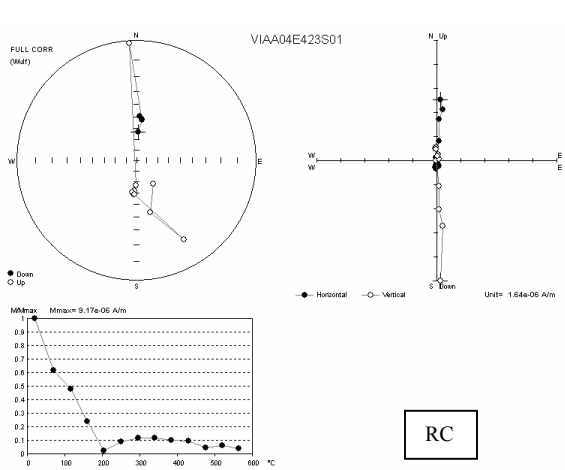

RC

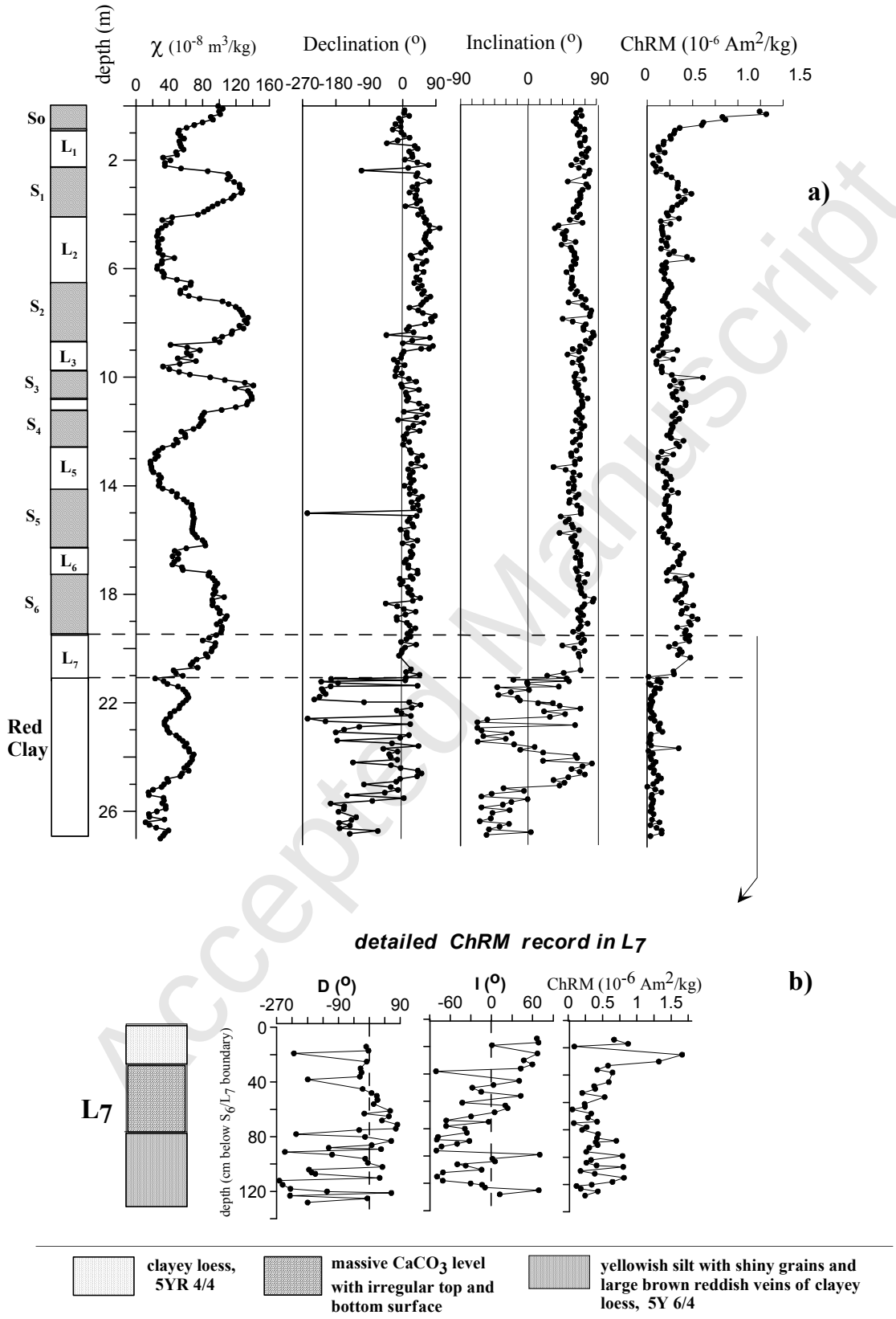

Figure 12

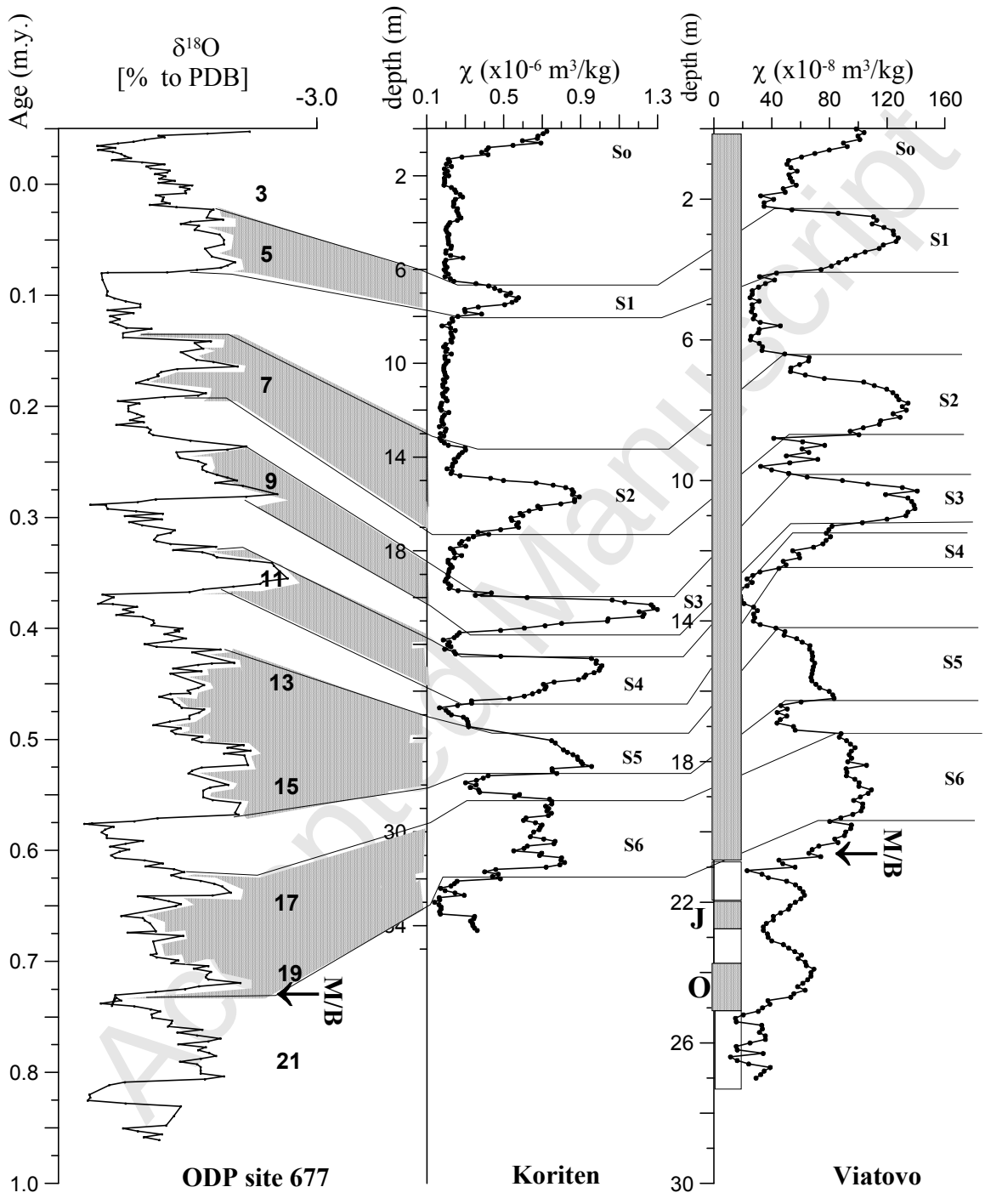

Figure 13

	Component 1			Component 2			Component 3		
	Rel. contr. (%)	$B_{1/2}$ (mT)	DP	Rel. contr. (%)	$B_{1/2}$ (mT)	DP	Rel. contr. (%)	$B_{1/2}$ (mT)	DP
So	67	34	0.28	26	83	0.29	7	582	0.53
loesses	33± 7	27± 2	0.24±0.02	53± 6	75± 11	0.3 ±0.02	13± 3	332±271	0.83± 0.13
palaeosols	51± 8	26± 1	0.23±0.01	34.5± 8	57± 9	0.32 ±0.01	13± 4	224±190	0.73± 0.13
All		**27± 3**	**0.24± .02**		**70 ± 12**	**0.32± 0.02**		**332±225**	**0.75±0.14**

Table 1

sample	unit	component 3		
		contribution (%)	B1/2 (mT)	DP(mT)
viaA01E120	L1	16	179.6	0.97
viaA01E490	L2	12	275	0.72
viaA02E060	L3	16	349.4	0.97
viaA02E240	L4	17	176.2	0.83
viaA02E500	L5	13	332	0.83
viaA02E790	L6	10	402.3	0.63
viaA03E370	L7	12	966.3	0.75
viaA01E300	S1	13	198.8	0.83
viaA01E780	S2	14	163.9	0.73
viaA02E130	S3	16	149.1	0.88
viaA02E280	S4	10	513.9	0.62
viaA02E660	S5	22	224.4	0.81
viaA03E090	S6	10	590.6	0.72
viaA04E250	RC	10	489.6	0.49
viaA01E020	So	7	581.7	0.53

Table 2

unit	N	Kmean (x10^{-6} SI)	L	F	P´	T
palaeosols	21	1491 (377.7)	1.001 (0.001)	1.002 (0.002)	1.004 (0.002)	0.396 (0.463)
loesses	10	555.9 (143)	1.001 (0.001)	1.003 (0.003)	1.004 (0.004)	0.27 (0.486)
Red clay	8	523.7 (337.9)	1.003 (0.002)	1.004 (0.002)	1.007 (0.003)	0.284 (0.297)

Table 3